Evening humid-heat maxima near the southern Persian/Arabian Gulf

Colin Raymond; Tom Matthews; Cascade Tuholske

communications earth & environment

Article

https://doi.org/10.1038/s43247-024-01763-3

Evening humid-heat maxima near the southern Persian/Arabian Gulf

Check for updates

Colin Raymond [1] ✉, Tom Matthews [2] & Cascade Tuholske [3,4]

Extreme humid heat is a major climate hazard for the coastal Arabian Peninsula. However, many of its characteristics, including diurnal and spatial variations, remain incompletely explored. Here we present evidence from multiple reanalysis and in situ datasets that evening or nighttime daily maxima in extreme wet-bulb temperature and heat index are widespread along the southern Persian/Arabian Gulf coastline and adjacent inland desert, driven principally by sea-breeze-related movements of moist maritime air. This timing runs counter to the general expectation of more intense heat and greater heat-stress risk during daytime hours. While wet-bulb temperature is one of many metrics relevant for understanding heat hazards, it has featured prominently in recent literature and its values are closer to uncompensable-heat limits in coastal Arabia than anywhere else. Deviations from an afternoon-peak assumption about heat risks are thus of critical importance and heighten the value of improved understanding of extreme-humid-heat meteorology, in this region and in others subject to similar physical processes.

The Arabian Peninsula is a region of exceptional and intensifying dry and humid heat[1–7]. Summertime near-surface air temperatures of 45–50 °C and sea-surface temperatures (SSTs) close to 35 °C are common[5,8,9]. Due primarily to anthropogenic climate change, temperatures are rising approximately 0.5 °C per decade and Persian/Arabian Gulf SSTs are rising 0.4 °C per decade, both rates being almost double the global average[3,8].

Consequently, there is strong evidence of serious and worsening heat-related health impacts in the region, including on mortality[10,11], labor[12,13], and religious and cultural activities[14], that together constitute a threat of cascading and increasingly unpredictable societal risks[15]. Even compared to the rest of the Middle East and North Africa region, Arabia is projected to see the largest percent increase in mortality over the 21st century[10]. Additionally, the theorized wet-bulb-temperature (Tw) deadly threshold of 35 °C, widely cited in the literature of the past decade[16,17], may be a major underestimation of health risks, particularly in low-humidity situations[7,18,19]. But regardless of precise thresholds or near-threshold health responses, Arabian Peninsula extreme events already closely approach both the dry and humid uncompensable-heat limits[5,16]—the most intense conditions in which human heat balance can be sustained indefinitely[20]. For these reasons, extreme heat is increasingly attracting scientific attention and governmental regulation in the region[12,21].

The primary elements of the Arabian summer climate include a seasonal anticyclone with large-scale subsidence, influenced by the South Asian summer monsoon and regional topography; high SSTs in the Red Sea and Persian/Arabian Gulf; and strong solar radiation[3,22]. These features combine to create a steep vertical gradient between a shallow boundary layer and the free troposphere, a gradient dominated by moisture: July mean specific humidity at the sea surface exceeds 20 g kg^{-1}, versus 4 g kg^{-1} only 200–300 m above[23]. This moisture, originating almost wholly from latent-heat fluxes over the Gulf, extends inland via sea breezes[9] and drives humid heat especially along the western and southern coasts[4,24]. The mean low-level wind is a northwesterly "shamal", superimposed on which is a ~1000-m-deep thermally driven circulation comprised of daytime sea breezes and nighttime land breezes[23,25]. The land breezes develop on almost every summer afternoon and evening[25], have a maximum near-surface speed on the Gulf's south coast, and can extend far inland, persisting through the overnight hours[23]. Near-surface wind direction thus greatly affects temperature and moisture, as do land-use modifications such as irrigation or urban development[24,26]. There is theoretical support for a strong relationship between Gulf SSTs and extreme heat in bordering land areas[5,9,17], and several past surveys have found empirical evidence of linkages between ocean and land due to a combination of shared processes and direct causality, but these have not focused on dynamics or the Middle East[27–29].

Extreme heat presents both daytime and nighttime risks[30], but in absolute terms is typically found (or assumed) to be more intense during the daytime hours[31–33], including in policies implemented in the study region[12]. In general, this is an excellent supposition, but it is precisely the rarity of the

[1]Joint Institute for Regional Earth System Science and Engineering, University of California, Los Angeles, Los Angeles, CA, USA. [2]Department of Geography, King's College London, London, UK. [3]Department of Earth Sciences, Montana State University, Bozeman, MT, USA. [4]Geospatial Core Facility, Montana State University, Bozeman, MT, USA. ✉e-mail: csraymond@ucla.edu

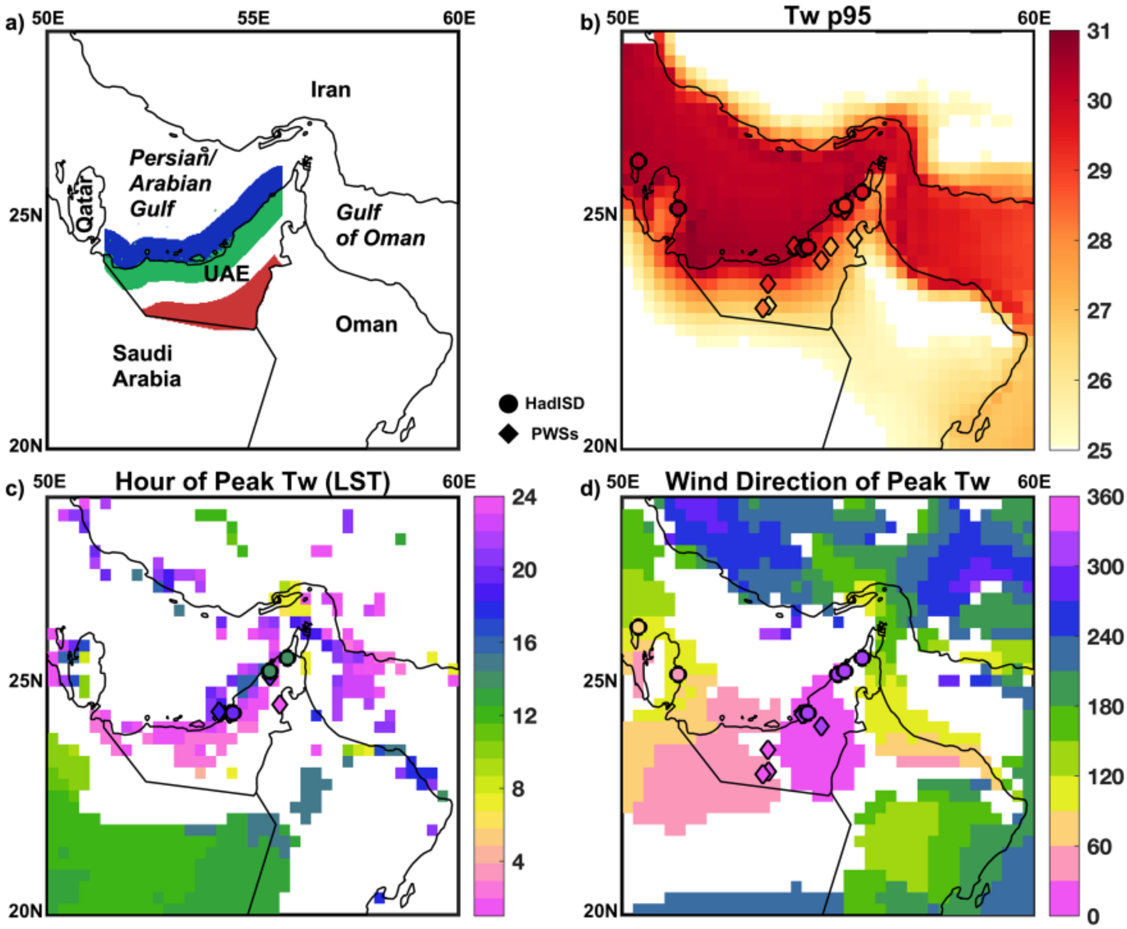

Fig. 1 | Key Tw characteristics in the southern Persian/Arabian Gulf. **a** Map of study region, including coastal-water (blue), coastal-land (green), and inland-desert (red) subregions. **b** Shading indicates the 95th percentile of Tw (°C) across all JJA days, 2000–2020, at each ERA5 gridcell. Symbols marking weather stations maintained by the UAE National Centre of Meteorology (circles) and personal weather stations (diamonds) use the same color scheme to represent the metric at those sites. **c** Hours (LST) for which a 6-hour surrounding window (see Methods) encompasses the largest number of >=95th-percentile daily-maximum Tw values, with a minimum of 50%. In blank areas, no hour meets this criterion. **d** Wind directions (°) for which a 90° surrounding window encompasses the largest number of >=95th-percentile daily-maximum Tw values, with a minimum of 50%. In blank areas, no direction meets this criterion.

potential exceptions to daytime peak heat extremes that interests us here. Recent evidence from South Asia reveals that the diurnal maximum of Tw occurs later in the day than the maximum (dry-bulb) temperature[34]. Most pertinently, the Tw maximum along the Arabian Sea coast of western India occurs at night, in association with shallow boundary-layer heights. A similar hint of evening humid heat is apparent from or mentioned in passing by previous work on Arabia[4,26], but this has not yet been validated, nor have the prevalence or processes been explored.

The goal of this study is to validate and extend these preliminary findings through assessment of four largely independent datasets, and to make sense of the results by placing them in regional meteorological context. While we focus on Tw, we evaluate and intercompare several humid-heat indices; these sharply differ in their sensitivity to humidity, among other characteristics, and there is no clear frontrunner in terms of relevance to impacts[35]. To support our analysis, we consider diurnal variations of humid heat, geographically and vertically, across the southern Persian/Arabian Gulf region centered on the United Arab Emirates (UAE).

We find that for some heat metrics, daily maxima of humid heat occur in the evening or nighttime hours in the coastal and inland-desert areas south of the Gulf. This phenomenon is driven by moisture anomalies, which are largest when the usual shallow sea-breeze circulation is intensified. Regional meteorological dynamics thus merit close attention if fine-grained heat exposure and associated risks—here and in climatologically similar regions—are to be accurately understood.

Results

Basic characteristics of extreme wet-bulb temperature

We consider results composited for three regions: the near-shore southern Persian/Arabian Gulf waters, the coastal UAE land, and the inland UAE desert (Fig. 1a). Over the Gulf and along its southern and western shorelines, 5% of all June-July-August (JJA) hours have a Tw above 31 °C (Fig. 1b), a critical value in laboratory tests[19] and exceptionally rare, or in fact above the all-time historical maximum, elsewhere in the world[4,36]. Moving inland from the coast in any direction, extreme Tw decreases rapidly (Fig. 1b). The European Centre for Medium-range Weather Forecasts Reanalysis 5 (ERA5) and weather stations agree well on these magnitudes, although with some disagreement in the inland desert.

As measured by Tw, the most common times of day at which these humid-heat extremes occur vary from midday in the inland deserts of Saudi Arabia, Oman, and Iran to evening or even nighttime in maritime and coastal areas (Fig. 1c). In the southernmost Persian/Arabian Gulf this diurnal cycle takes the form of an over-water peak around 8 pm local standard time (LST); by midnight the peak has shifted to the coastal land, and then further south into the UAE interior by the early-morning hours. A similar geographic shift through the course of the day is seen on the western Gulf coast near Qatar, and the northern Gulf coast of southern Iran. Hadley Integrated Surface Database (HadISD) weather stations and personal weather stations (PWSs) help corroborate ERA5's evening peak for the UAE central coast near Abu Dhabi, and its midnight peak for the inland desert

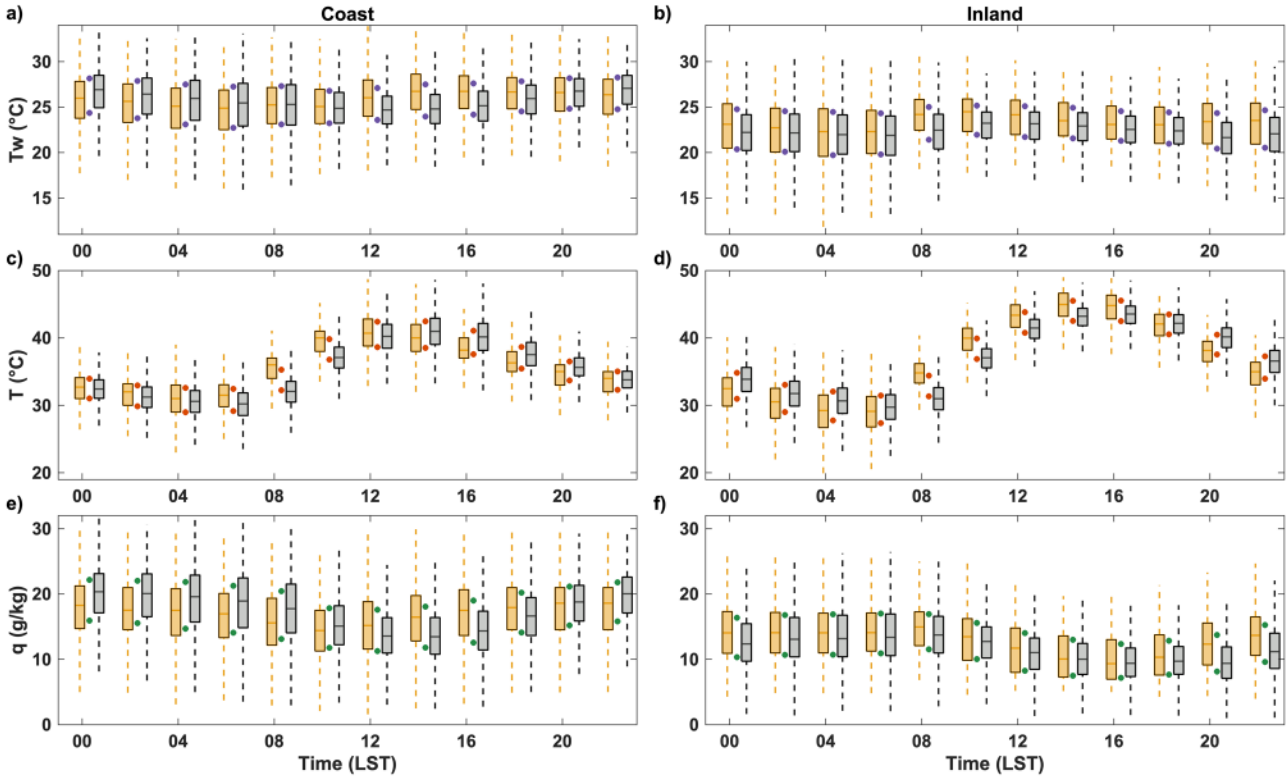

Fig. 2 | Reanalysis and weather-station diurnal ranges of humid-heat-related variables. **a** Distribution of 2 m Tw for coastal-land ERA5 gridcells (gray) and weather stations (gold) by hour for JJA, with only even-numbered hours shown for clarity. To aid in visual assessment, dots mark the ERA5/station mean for the tops (75th percentile) and bottoms (25th percentile) of the boxes. **b** As in (**a**) but for the inland-desert subregion. **c**, **d** As in (**a**, **b**) but for 2 m temperature. **e**, **f** As in (**a**, **b**) but for 2 m specific humidity.

near Al Ain. On the eastern UAE coast near Dubai and Ras al-Khaimah, a discrepancy of the peak timing is observed between ERA5 (evening) and HadISD stations (afternoon).

ERA5 wind directions at the time of maximum Tw indicate onshore flow throughout the Gulf region (Fig. 1d). Especially notable is the interstitial space in the Rub' al Khali (near the UAE-Saudi Arabia-Oman tripoint) where humid air masses from the south, east, and north collide, with only spatial bands <100 km wide being subject to multiple regimes. Weather stations, particularly first-order ones located at airports, generally agree with this picture too, as do all PWSs of sufficient quality for inclusion.

Examining the diurnal cycle for UAE coastal and inland locations, ERA5 presents Tw as being slightly higher in nighttime than daytime (Fig. 2a, b). On the highest-Tw days, the timing of the Tw minimum progresses from midday along the coast to late afternoon, evening, or overnight in the inland desert, in contrast to below-average JJA days which see a sharper minimum around dawn. The pronounced daytime minimum of specific humidity in both regions appears to primarily drive these patterns, partially counterbalanced by the daytime maximum of temperature. Relative to weather stations, and especially for hot days, ERA5 has too muted of a diurnal cycle, with notable underestimates of temperature during the morning to early-afternoon hours, and of specific humidity from midday into evening.

Multivariate and meteorological analysis of humid heat

To gain further insight into the synoptic meteorology of humid heat near the Persian/Arabian Gulf south coast, we compare Tw with several other humid-heat metrics, and also consider co-occurring values of related meteorological quantities. We again see that over water Tw values are high and have little diurnal variation, while over land an afternoon maximum in temperature is more than offset, in terms of Tw, by a nadir in specific humidity (Fig. 3a, e, f). The Universal Thermal Climate Index (UTCI) and wet-bulb globe temperature (WBGT), which additionally account for solar radiation and wind speed, retain a more typical daytime peak on both hot-humid days and all other warm-season days (Fig. 3b, c). However, the diurnal cycle of the heat index, and its relative values in the different regions, is similar to that of Tw.

Together, Figs. 3 and 4 reveal the reasons for the varying heat magnitudes and timing along a coast-interior transect. At the coast, temperature begins to fall and specific humidity to rise in mid-afternoon, coincident with increasing onshore wind speed, causing a clear separation from the conditions of the inland desert (Figs. 3 and 4). Our results parallel prior ones[25] in the timing of this coastal temperature maximum, and in an evening speed maximum of the sea breeze, which then slackens close to midnight. But the anomalous advected moisture lingers inland until morning (Fig. 4), when a deepening boundary layer helps disperse it and offshore winds sweep it back over the Gulf (Fig. 3). Earlier work[26] has shown a similar timing and inland extent of nighttime moisture, even anticipating such features as the very shallow boundary layer[4]. The difference between high-temperature and high-Tw days (as defined for Abu Dhabi) lies principally in the strong and sustained low-level onshore flow on the latter, especially in the evening to post-midnight hours (Fig. 4). The former set of days see night and morning offshore downslope winds at the coast, typical for the region in summer[23], while for the latter set this feature is weak to non-existent.

We lastly consider diurnal variations in the vertical structure of temperature and moisture among the three study regions. Most of the diurnal change, as well as nearly all the difference between the seasonal mean and hot-humid days, takes place below 925 hPa (approximately 800 m) (Fig. 5). Temperatures on hot-humid days are near normal, while specific humidity has a large positive anomaly[37]. Variations are generally larger farther from the coast. All data sources broadly concur on the overall vertical structure of Tw on both sets of days, although there are some discrepancies at the lowest

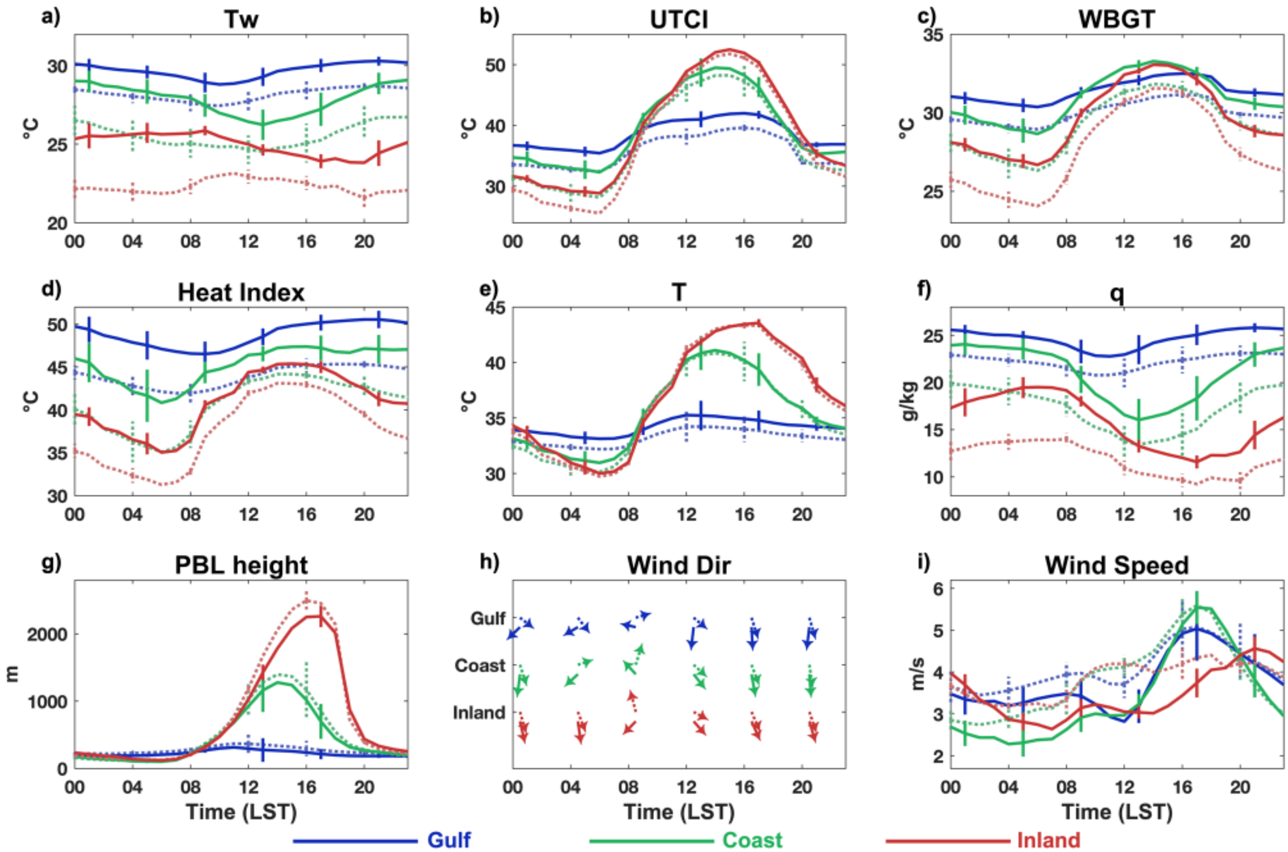

Fig. 3 | Diurnal composites of several humid-heat metrics and related variables. **a** Diurnal composite of Tw (°C) on all JJA days (dotted) and on hot-humid days (solid), for selected ERA5 gridcells in the coastal-water (blue), coastal-land (green), and inland-desert (red) subregions. Error bars represent ±1 standard deviation. **b–i** As in (**a**) but for UTCI (°C); WBGT (°C); heat index (°C); 2 m temperature (°C); 2 m specific humidity (g/kg); planetary-boundary-layer height (m); wind direction; and wind speed (m/s).

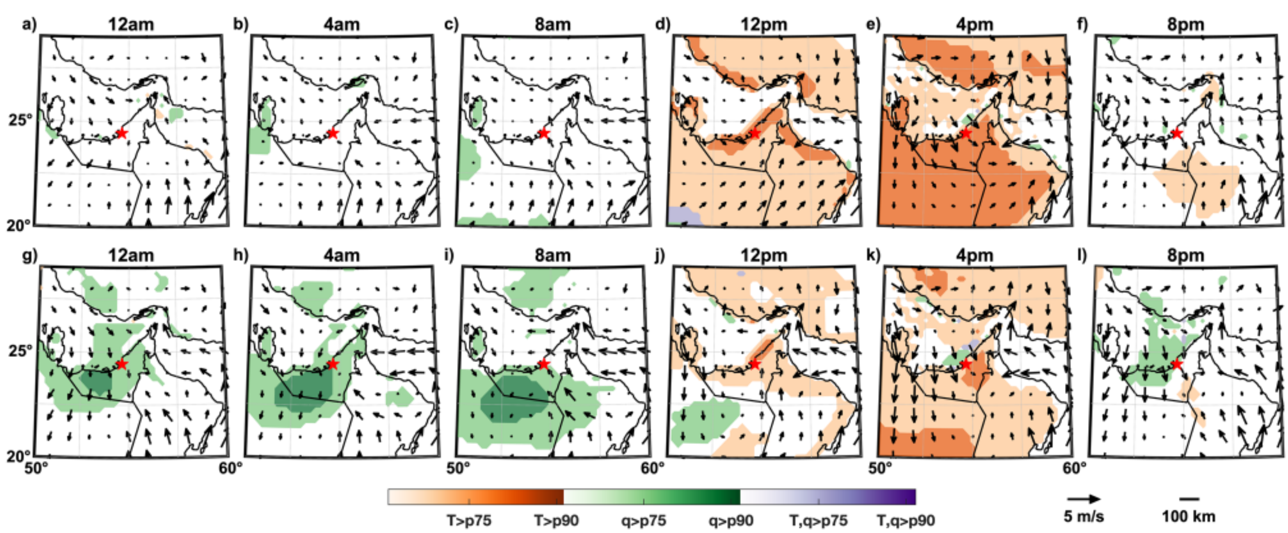

Fig. 4 | Spatiotemporal assessment of high-temperature and high-Tw days. **a–f** The composited diurnal cycle of temperature, specific humidity, and wind for all days which at any hour exceeded the gridcell 95th percentile of temperature. Temperature and specific humidity are shown as binary exceedances of gridcell 75th and 90th percentiles, with exceedances of a certain percentile in both variables simultaneously shown in purple. Winds are actual (non-anomaly). Times are LST. **g–l** As in (**a–f**) but for days exceeding the 95th percentile of Tw (i.e., hot-humid days).

level: HadISD weather-station data at Abu Dhabi indicate a gradual increase in Tw through the afternoon, with a peak around 8 pm LST, while ERA5 has a similar increase displaced several hours later, spanning roughly 4 pm to midnight (Fig. 5). Radiosondes tend to support the weather-station view, above all for the afternoon hours.

Discussion

The climate of coastal southeastern Arabia, and especially the details of its humid-heat extremes, depends strongly on the low-level flow. Sustained onshore winds advect the perennially high moisture of the Persian/Arabian Gulf boundary layer over land[3,9], resulting in the unusual combination of

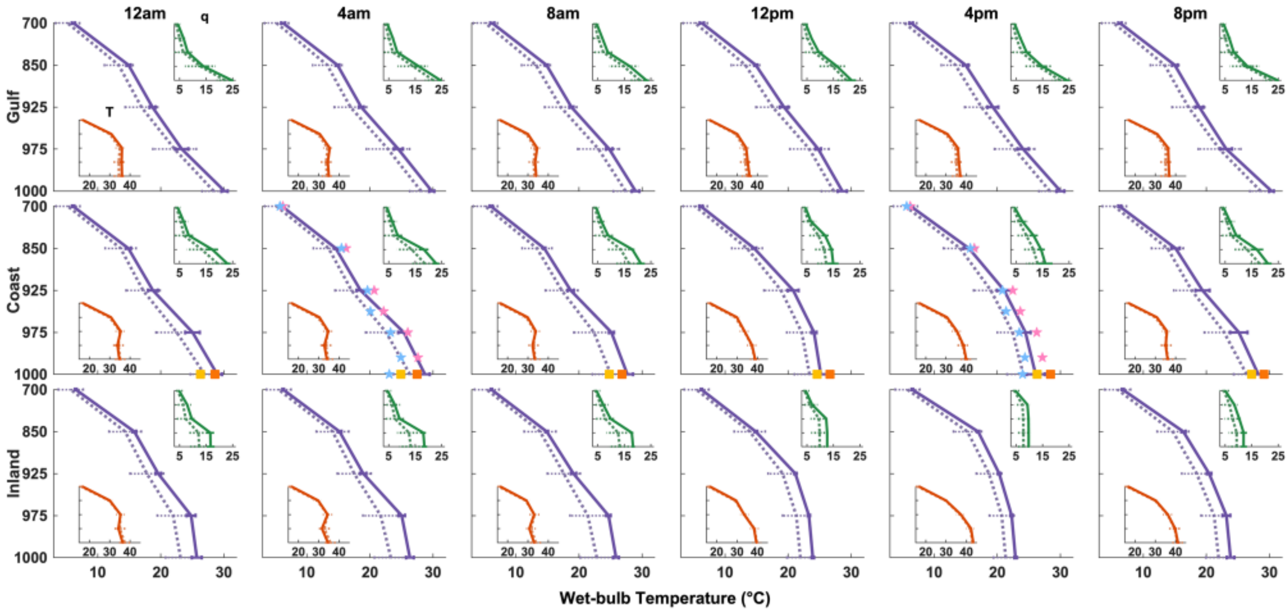

Fig. 5 | Temperature and moisture vertical profiles and their combined effect on humid heat. (Large plots) Vertical profiles of Tw on all JJA days (purple, dashed) and on hot-humid days (purple, solid), composited for ERA5 gridcells in each subregion (rows) and times of day (LST, columns). Error bars represent ±1 standard deviation. For all subplots, y-axes represent pressure levels (hPa). Pink (blue) stars indicate Tw on pressure levels from Abu Dhabi radiosondes for all (hot-humid) days. Orange (yellow) squares indicate the same variables at 2 m from the Abu Dhabi Airport weather station. Insets at lower left: as in large plots but for temperature (°C). Insets at upper right: as in large plots but for specific humidity (g/kg).

elevated specific humidity and negligible temperature anomalies (Figs. 3, 4, 5)[4,24,37]. The timing and magnitude of diurnal specific-humidity variations is closely connected to the speed and directionality of the low-level wind (Figs. 1, 3, 4; Supplementary Figs. 1, 2), a factor which appears to also substantially explain the ERA5/station discrepancies along the coast shown in Fig. 2: ERA5 has a weak and delayed-onset onshore wind relative to weather stations, causing specific humidity to erroneously decrease for several additional midday hours (Supplementary Fig. 2). The maritime-air effect can also be traced through its signature of low boundary-layer heights. These sea breezes, or more precisely their air-mass influence, can reach well over 100 km inland, in some cases 250 km or more (Fig. 4)[23,25,38]. Their timing, direction, and overall spatial pattern as found here are broadly consistent with previous work[23,25] and correspond closely to periods of elevated Tw across a coast-to-interior continuum (Figs. 3 and 4). The combination of land breeze and katabatic flow that dominates the nighttime circulation in the southern Persian/Arabian Gulf region during much of the summer[23,38] is conspicuously absent on hot-humid nights (Fig. 4), another sign of the importance of maritime influence.

Reanalysis, weather stations, and radiosondes are in broad agreement about the magnitude and timing of extreme Tw, and about what sets days on which it occurs apart from the already hot and humid summertime regional mean. Like Tw, the heat index exhibits an evening or nighttime maximum on hot-humid days (versus a slight afternoon maximum otherwise), while the UTCI and WBGT do not, as they include solar radiation and are also more sensitive to temperature. Even so, large humidity anomalies on hot-humid days keep WBGT in the 'light workload' category along the coast in the evening and through most of the night (Fig. 3)[39,40], carrying the additional potential of sleep disruption for populations lacking access to reliable artificial cooling[41]. That the highest values of Tw and heat index at all hours, and of UTCI and WBGT at night, are located over the Gulf waters (Figs. 1, 3) implies considerable dangers for those with maritime occupations, such as fishers, mariners, and oil-platform workers[42]. Very high specific humidity can also raise health concerns on its own, such as a link with respiratory mortality in southern China likely due to a combination of breathing difficulties, increased infections, and broadly elevated heat-stress risk[43].

The metrics analyzed in this study—Tw, heat index, UTCI, WBGT, and air temperature—are but a subset of the dozens of heat indicators that have been developed, which differ in variables included and in their weighting[44]. The suitability of a given metric for quantifying impacts to human health and wellbeing is difficult to determine other than in broad strokes, as heat risk is a function of multitudinous variations in physiology, exposure, meteorology, and other factors[18]. For example, a person along the southern Persian/Arabian Gulf coast who is exposed to the sun would likely experience an afternoon heat-risk peak when accounting for radiation via the UTCI and WBGT (Fig. 3b, c), whereas a person in shaded conditions or indoors (situations more closely characterized by Tw and heat index) would experience an evening peak (Fig. 3a, d)[18,19,45]. Such differences, which gloss over myriad other disparities in metric behavior, complicate simple population-level conclusions firmly connecting overall humid-heat risk to particular humid-heat metrics[35,46]. Impact assessments must be cognizant of these uncertainties and, if possible, ensure that chosen metrics align with the impacts or subpopulations under consideration[18,40,44]. In this study we focus on Tw partly in dialogue with recent literature[5,7,14,16–19,26,34–36,46,47] and partly because it is proportional to total heat content[4], making the statement 'coastal heat peaks in the evening hours' physically true—although there remains considerable uncertainty about the extent to which that statement also holds for thermal sensation.

Metric choice is not the only source of difference or uncertainty around representing humid heat in the Middle East. However, our study reinforces most prior evidence in terms of the spatial and temporal characteristics of the highest Tw. At least one study[7] located the spatial maximum in the northern Persian/Arabian Gulf waters and along the southern Iran coast, whereas other modeling studies as well as reanalysis- and observation-based datasets (including ERA5) largely place the maximum in the southern portion, along the UAE and/or Qatar coast (Fig. 1; Supplementary Fig. 3)[5,16,17,48]. Dataset uncertainty is also apparent temporally. For example, at the lowest vertical level in Fig. 5, ERA5 likely overestimates the amount of diurnal variation in Tw at the coast, placing the peak Tw around midnight LST versus the in-situ indication of approximately 8 pm. It is unclear in such cases which data source, if either, may be considered more reliable, especially in connection with the inherent difficulties of representing steep gradients in temperature and moisture that span only a few gridcells (Fig. 1). In any case, we argue that the resulting uncertainty is not so large as to threaten the conclusion of Tw (and heat index) reaching its maxima in the post-sunset hours for much of the coastal land around the southern Gulf (Fig. 1). On the Gulf's north shore, a prior case study[49] found midday Tw maxima during a 2015 heat event at Bandar Mahshahr, Iran, a finding replicated here when we replot Fig. 1 over a larger domain (Supplementary Fig. 3). But even that timeseries, for a location nearly 1000 km away and on the opposite side of the Gulf from our study region, contains several Tw values quite close to the daily maximum in the evening or late-night hours.

Under continued global warming, substantial future increases of Tw are expected in Arabia, of similar magnitude day and night[26]. Because of the climatological intensity of humid heat in the region, with even non-peak readings of all humid-heat metrics regularly reaching 'danger' categories, heat-stress implications are serious for even moderate warming levels[1,18]. In the southern Persian/Arabian Gulf, most recent development is located along the coast[47], heightening exposure to the humid-heat hazard. Further interrogation of hazard drivers at subseasonal timescales, such as feedbacks involving coastal marine heatwaves and their atmospheric effects[27,29], will aid in providing nuance and interpretation to our findings, and can facilitate the development of fine-grained metrics and warning systems.

The essential conclusion we report here is that excessive levels of maritime moisture in this otherwise arid region can dominate the diurnal cycle of humid-heat metrics like Tw to the point of almost entirely inverting it. This counterintuitive phenomenon is particularly relevant to shaded conditions either indoors or outdoors, and makes further examination of the spatiotemporal patterns of humid-heat intensity, including their driving processes, of crucial importance for the accurate assessment of local heat risk.

Methods

Datasets

We use hourly data for JJA 2000–2020 from the 0.25°-resolution ERA5 reanalysis[50–52]; from 6 weather stations in the HadISD network, v3.4.0.2023f[53,54]; and from 12 PWSs in the WeatherUnderground.com network. Analyzed HadISD and PWS data (see Supplementary Tables 1 and 2) are only from those stations which meet the minimum-sample-size requirement of 100 days. PWSs are unvalidated and often of limited duration, but are included here due to the value provided by their wide geographic coverage compared to other in situ sources. We also use data from the Radiosounding HARMonization dataset[55,56], available daily at 00 and 12 UTC, though our focus region of the southern Arabian Peninsula contains only one regular radiosonde location (Abu Dhabi).

Analysis variables

The principal variables obtained are air (dry-bulb) temperature and specific humidity, from which we calculate Tw at 2 m and at 1000, 975, 925, 850, and 700 hPa[57]. From ERA5 we also obtain wind direction and speed, planetary-boundary-layer height, and several radiation quantities needed to calculate mean radiant temperature: surface net short-wave, surface net long-wave, surface short-wave downwards, surface long-wave downwards, and total-sky direct. While Tw serves as our primary humid-heat metric, for comparison purposes we assess the US National Weather Service heat index[58], UTCI[59], and WBGT[39].

Humid-heat definition

To define hot-humid days, we first compute the 95th percentile of Tw across all 2000–2020 JJA hours at each gridcell or in situ location, then find those days with at least one hour exceeding the local 95th percentile. We term these "hot-humid days" and they encompass approximately 15-20% of all JJA days. Our intention with this approach is to allow for all hours to be readily compared against one another in terms of the probability of reaching a locally extreme value. Composite means for the diurnal cycle on hot-humid days are then calculated for every metric.

Peak hours

For all hot-humid days, we compute at each gridcell the hour of the daily maximum Tw. We term the mode of this distribution a 'peak hour' if >=50% of values occur within a 6-h surrounding window, i.e. within 3 h on either side. Gridcells whose daily maxima are not concentrated at any particular time of day are thus considered to have no peak hour. An analogous calculation is also done for wind direction, with the requirement of wind direction being within 45° of the peak direction. The robustness of the results of Fig. 1 to definitional changes is evaluated by reducing the minimum window fraction from 50% to 40% (Supplementary Fig. 4) and by assessing peak hours for the heat index, UTCI, and WBGT (Supplementary Fig. 5).

Data availability

The processed data arrays necessary to reproduce all manuscript figures have been published at doi:10.6084/m9.figshare.27058477. ERA5 and Radiosounding HARMonization datasets are available from the Copernicus Climate Change Service Climate Data Store[51,52,56]. HadISD station data[53,54] are available from https://www.metoffice.gov.uk/hadobs/hadisd/v340_2023f/index.html, and PWS data from https://www.wunderground.com/wundermap.

Code availability

All code used in data processing and figure creation has been made available through a Zenodo repository[60]. Code was written and tested using MATLAB R2023a.

Received: 7 February 2024; Accepted: 3 October 2024;
Published online: 14 October 2024

References

1. Vecellio, D. J., Kong, Q., Kenney, W. L. & Huber, M. Greatly enhanced risk to humans as a consequence of empirically determined lower moist heat stress tolerance. *Proc. Natl. Acad. Sci. USA* **120**, e2305427120 (2023).
2. Speizer, S., Raymond, C., Ivanovich, C. & Horton, R. M. Concentrated and intensifying humid heat extremes in the IPCC AR6 regions. *Geophys. Res. Lett.* **49**, e2021GL097261 (2022).
3. Zittis, G. et al. Climate change and weather extremes in the Eastern Mediterranean and Middle East. *Rev. Geophys.* **60**, e2021RG000762 (2022).
4. Raymond, C. et al. On the controlling factors for globally extreme humid heat. *Geophys. Res. Lett.* **48**, e2021GL096082 (2021).
5. Raymond, C., Matthews, T. K. & Horton, R. M. The emergence of heat and humidity too severe for human tolerance. *Sci. Adv.* **6**, eaaw1838 (2020).
6. Lelieveld, J. et al. Strongly increasing heat extremes in the Middle East and North Africa (MENA) in the 21st century. *Clim. Change* **137**, 245–260 (2016).
7. Pal, J. S. & Eltahir, E. A. B. Future temperature in southwest Asia projected to exceed a threshold for human adaptability. *Nat. Clim. Change* **6**, 197–200 (2016).
8. Alosairi, Y., Alsulaiman, N., Rashed, A., & Al-Houti, D. World record extreme sea surface temperatures in the northwestern Arabian/Persian Gulf verified by in situ measurements. *Mari. Poll. Bull.* **161**, 111766 (2020).
9. Xue, P. & Eltahir, E. A. B. Estimation of the heat and water budgets of the Persian (Arabian) Gulf using a regional climate model. *J. Clim.* **28**, 5041–5062 (2015).
10. Hajat, S., Proestos, Y., Araya-Lopez, J.-L., Economou, T. & Lelieveld, J. Current and future trends in heat-related mortality in the MENA region: A health impact assessment with bias-adjusted statistically downscaled CMIP6 (SSP-based) data and Bayesian inference. *Lancet Planet. Health* **7**, e282–e290 (2023).

11. Pradhan, B. et al. Heat stress impacts on cardiac mortality in Nepali migrant workers. *Cardiol* **143**, 37–48 (2019).
12. Flouris, A. D. et al. Assessment of occupational heat strain and mitigation strategies in Qatar. Report of the International Labour Organization Project Office in Qatar (2019). Report number FL/2019/13.
13. Al-Bouwarthan, M., Quinn, M. M., Kriebel, D. & Wegman, D. H. Assessment of heat stress exposure among construction workers in the hot desert climate of Saudi Arabia. *Ann. Work Exposur. Health* **63**, 505–520 (2019).
14. Kang, S., Pal, J. S. & Eltahir, E. A. B. Future heat stress during Muslim pilgrimage (Hajj) projected to exceed "extreme danger" levels. *Geophys. Res. Lett*. **46**, 10094–10100 (2019).
15. Lahn, G. & Shapland, G. Cascading climate risks and options for resilience and adaptation in the Middle East and North Africa. Report of the Cascading Climate Impacts Project. 122 pp. (2022). Retrieved from https://www.cascades.eu/publication/cascading-climate-risks-and-options-for-resilience-and-adaptation-in-the-middle-east-and-north-africa/.
16. Powis, C. M. et al. Observational and model evidence together support wide-spread exposure to noncompensable heat under continued global warming. *Sci. Adv*. **9**, eadg9297 (2023).
17. Buzan, J. R. & Huber, M. Moist heat stress on a hotter Earth. *Ann. Rev. Earth Planet. Sci*. **48**, 623–655 (2020).
18. Vanos, J. et al. A physiological approach for assessing human survivability and liveability to heat in a changing climate. *Nat. Commun*. **14**, 7653 (2023).
19. Vecellio, D. J., Wolf, S. T., Cottle, R. M. & Kenney, W. L. Evaluating the 35C wet-bulb temperature adaptability threshold for young, healthy subjects (PSU HEAT Project). *J. Appl. Physiol.* **132**, 340–345 (2022).
20. Cottle, R. M., Lichter, Z. S., Vecellio, D. J., Wolf, S. T. & Kenney, W. L. Core temperature responses to compensable versus uncompensable heat stress in young adults (PSU HEAT Project). *J. Appl. Physiol.* **133**, 1011–1018 (2022).
21. Qatar Ministry of Labour. Heat stress legislation in Qatar: A guide for employers. Issued May 24, 2020. 32 pp. (2022). Accessed from https://www.ilo.org/wcmsp5/groups/public/---arabstates/documents/genericdocument/wcms_794519.pdf.
22. Tyrlis, E., Lelieveld, J. & Steil, B. The summer circulation over the eastern Mediterranean and the Middle East: Influence of the South Asian monsoon. *Clim. Dynam.* **40**, 1103–1123 (2013).
23. Zhu, M. & Atkinson, B. W. Observed and modelled climatology of the land-sea breeze circulation over the Persian Gulf. *Int. J. Clim.* **24**, 883–905 (2004).
24. Ivanovich, C., Anderson, W., Horton, R., Raymond, C. & Sobel, A. The influence of intraseasonal oscillations on humid heat in the Persian Gulf and South Asia. *J. Clim.* **35**, 4309–4329 (2022).
25. Eager, R. E. et al. A climatological study of the sea and land breezes in the Arabian Gulf region. *J. Geophys. Res.* **113**, D15106 (2008).
26. Safieddine, S., Clerbaux, C., Clarisse, L., Whitburn, S. & Eltahir, E. A. B. Present and future land surface and wet bulb temperatures in the Arabian Peninsula. *Environ. Res. Lett.* **17**, 044029 (2022).
27. Hu, L. A global assessment of coastal marine heatwaves and their relation with coastal urban thermal changes. *Geophys. Res. Lett*. **48**, 10.1029/2021GL093260 (2021).
28. Karmalkar, A. V. & Horton, R. M. Drivers of exceptional coastal warming in the northeastern United States. *Nat. Clim. Change* **11**, 854–860 (2021).
29. Pathmeswaran, C., Sen Gupta, A., Perkins-Kirkpatrick, S. E. & Hart, M. A. Exploring potential links between co-occurring coastal terrestrial and marine heatwaves in Australia. *Front. Clim*. **4**, https://doi.org/10.3389/fclim.2022.792730 (2022).
30. Tao, J. et al. Daytime and nighttime high temperatures differentially increased the risk of cardiovascular disease: A nationwide hospital-based study in China. *Environ. Res*. **236**, 116740 (2023).
31. Wouters, H. et al. Soil drought can mitigate deadly heat stress thanks to a reduction of air humidity. *Sci. Adv*. **8**, eabe6653 (2022).
32. Chakraborty, T., Venter, Z. S., Qian, Y. & Lee, X. Lower urban humidity moderates outdoor heat stress. *AGU Adv*. **3**, e2022AV000729 (2022).
33. Raymond, C., Singh, D. & Horton, R. M. Spatiotemporal patterns and synoptics of extreme wet-bulb temperature in the contiguous United States. *J. Geophys. Res. Atmos.* **122**, 13108–13124 (2017).
34. Justine, J., Monteiro, J. M., Shah, H. & Rao, N. The diurnal variation of wet bulb temperatures and exceedance of physiological thresholds relevant to human health in South Asia. *Nat. Commun. Earth Environ.* **4**, 244 (2023).
35. Simpson, C. H., Brousse, O., Ebi, K. L. & Heaviside, C. Commonly used indices disagree about the effect of moisture on heat stress. *npj Clim. Atmos. Sci*. **6**, 78 (2023).
36. Rogers, C. D. W. et al. Recent increases in exposure to extreme humid-heat events disproportionately affect populated regions. *Geophys. Res. Lett*. **48**, e2021GL094183 (2021).
37. Ivanovich, C., Raymond, C., Sobel, A. & Horton, R. Stickiness: A new variable to characterize the temperature and humidity contributions toward humid heat. *J. Atmos. Sci.* **81**, 819–837 (2024).
38. Warner, T. T. & Sheu, R.-S. Multiscale local forcing of the Arabian Desert daytime boundary layer, and implications for the dispersion of surface-released contaminants. *J. Appl. Meteorol.* **39**, 686–707 (2000).
39. Brimicombe, C. et al. Wet bulb globe temperature: Indicating extreme heat risk on a global grid. *GeoHealth*, **7**, e2022GH000701 (2023).
40. Foster, J. et al. An advanced empirical model for quantifying the impact of heat and climate change on human physical work capacity. *Int. J. Biometeorol.* **65**, 1215–1229 (2021).
41. Obradovich, N., Migliorini, R., Mednick, S. C. & Fowler, J. H. Nighttime temperature and human sleep loss in a changing climate. *Sci. Adv*. **3** (2021).
42. Kjellstrom, T., Freyberg, C., Lemke, B., Otto, M. & Briggs, D. Estimating population heat exposure and impacts on working people in conjunction with climate change. *Int. J. Biometeorol.* **62**, 291–306 (2018).
43. Chen, S. et al. The role of absolute humidity in respiratory mortality in Guangzhou, a hot and wet city of South China. *Env. Health Prev. Med.* **26**, 109 (2021).
44. Ioannou, L. G. et al. Indicators to assess physiological heat strain—Part 3: Multi-country field evaluation and consensus recommendations. *Temperature* **9**, 274–291(2022).
45. Lu, Y.-C. & Romps, D. M. Predicting fatal heat and humidity using the heat index model. *J. Appl. Physiol.* **134**, 649–656 (2023).
46. Baldwin, J. W. et al. Humidity's role in heat-related health outcomes: A heated debate. *Environ. Health Persp*. **131**, 55001 (2023).
47. Bolleter, J., Grace, B., Hooper, P. & Foster, S. Wet-bulb temperature and sea-level rise in the United Arab Emirates — Planning responses. *Plan. Pract. Res.* **36**, 408–429 (2021).
48. Suarez-Gutierrez, L., Müller, W. A., Li, C. & Marotzke, J. Hotspots of extreme heat under global warming. *Clim. Dynam.* **55**, 429–447 (2020).
49. Schär, C. The worst heat waves to come. *Nat. Clim. Change* **6**, 128–129 (2016).
50. Hersbach, H. et al. The ERA5 global reanalysis. *Q. J. R. Meteorol. Soc.* **146**, 1999–2049 (2020).
51. Hersbach, H. et al. ERA5 hourly data on single levels from 1940 to present. Copernicus Climate Change Service (C3S) Climate Data Store (CDS). https://doi.org/10.24381/cds.adbb2d47. Accessed 2023-11-10.
52. Hersbach, H. et al. ERA5 hourly data on pressure levels from 1940 to present. Copernicus Climate Change Service (C3S) Climate Data

Store (CDS). https://doi.org/10.24381/cds.bd0915c6. Accessed 2023-11-10.
53. Dunn, R. J. H., Willett, K. M., Parker, D. E. & Mitchell, L. Expanding HadISD: quality-controlled, sub-daily station data from 1931. *Geosci. Instrum. Method. Data Syst.* **5**, 473–491 (2016).
54. Smith, A., Lott, N. & Vose, R. The Integrated Surface Database: Recent developments and partnerships. *Bull. Amer. Meteorol., Soc.* **92**, 704–708 (2011).
55. Madonna, F. et al. The new Radiosounding HARMonization (RHARM) data set of homogenized radiosounding temperature, humidity, and wind profiles with uncertainties. *J. Geophys. Res. Atmos*. **127**, e2021JD035220 (2022).
56. Durre, I., Xungang, Y., Vose, R. S., Applequist, S. & Arnfield, J. Integrated Global Radiosonde Archive (IGRA), version 2. NOAA National Centers for Environmental Information. https://doi.org/10.7289/v5x63k0q. Accessed 2023-12-02.
57. Davies-Jones, R. An efficient and accurate method for computing the wet-bulb temperature along pseudoadiabats. *Mon. Wea. Rev.* **136**, 2764–2785 (2008).
58. Rothfusz, L. P. The heat index "equation" (or, more than you ever wanted to know about heat index). Technical Attachment (SR 90-23), National Weather Service (1990).
59. Jendritzky, G., de Dear, R. & Havenith, G. U. T. C. I. Why another thermal index? *Int. J. Biometeorol.* **56**, 421–428 (2012).
60. Raymond, C. MATLAB code for "Evening humid-heat maxima near the southern Persian/Arabian Gulf." https://doi.org/10.5281/zenodo.13787910. Updated 2024-09-17.

Acknowledgements
C.R. and C.T. were supported by the NASA Land-Cover and Land-Use Change Program grant no. 80NSSC23K0525.

Author contributions
C.R. conceptualized the research, performed the research, and wrote and revised the paper. T.M. conceptualized the research and wrote and revised the paper. C.T. wrote and revised the paper.

Competing interests
The authors declare no competing interests.

Additional information
Supplementary information The online version contains supplementary material available at https://doi.org/10.1038/s43247-024-01763-3.

Correspondence and requests for materials should be addressed to Colin Raymond.

Peer review information *Communications Earth and Environment* thanks the anonymous reviewers for their contribution to the peer review of this work. Primary Handling Editors: Min-Hui Lo, Heike Langenberg. A peer review file is available.